Journal of Electroceramics, 9, 155–164, 2002

Featured Article: Use of Microhotplates in the Controlled Growth and Characterization of Metal Oxides for Chemical Sensing

R.E. CAVICCHI, S. SEMANCIK, F. DiMEO JR. & C.J. TAYLOR
Chemical Science and Technology Laboratory, National Institute of Standards and Technology, Gaithersburg, MD 20899, USA

Submitted April 19, 2002; Accepted January 6, 2003

Abstract. Microhotplates are micromachined platforms with integrated heaters and contact electrodes that can be used as miniature substrates for metal oxide film growth. Fabricated as arrays, they enable efficient combinatorial studies to be performed on a single chip. A variety of growth methods are compatible with their use, including evaporation, sputtering, chemical vapor deposition, and deposition from pastes or sol gels using screen printing, drop deposition, or spin-coating. The microheater on each element may be used to control the temperature during deposition or for a post-annealing step such as sintering, while the film contact electrodes serve as a built-in monitor of the fabrication process. In chemical vapor deposition using arrays, the elements with heaters set above the lowest nucleation temperature for a given precursor are the only ones that will have film deposited on them, resulting in a kind of self-lithography. This review gives examples of different methods of film growth that have been employed on microhotplates with applications for chemical sensing, with an emphasis on the chemical vapor deposition method.

Keywords: gas sensor, microhotplate, membrane, micromachined, chemical vapor deposition, tin oxide

1. Introduction

Among the different classes of gas sensors, devices based on conductance changes of metal oxides find wide application because of their sensitivity, reversibility, speed, robustness, and low cost. Elevated temperatures (200–500°C) are required to optimize the performance of these materials. Initially motivated by the goal of minimizing the power required for a device to reach these temperatures [1, 2], device research over the past decade has focused on the use of microfabrication and micromachining to make arrays of small devices with integrated heaters, thermometers and sensors [3–5]. For sensing, additional benefits accrue from this microfabrication approach. Arrays can be produced with different materials on different elements or operated at different temperatures to produce a system response which is different for different gases, overcoming the lack of chemical selectivity from individual elements [6–10]. The small size allows rapid heating and cooling so that temperature modulation may be used to enhance the chemical selectivity of individual elements [11, 12]. The fabrication methods can be made compatible with CMOS (complementary metal oxide semiconductor) processing used to produce conventional integrated circuits so that functionalities such as signal processing and multiplexing can be performed on the same chip as the sensors [13, 14].

Microhotplates also open up new possibilities for metal oxide film fabrication that are not available in conventional wafer-scale film growth. These arise from the ability to use the microheater on each array element can be to control the growth or processing of the film on that element [15, 16]. Localized control means different array elements on the same chip can be given different thermal histories during the film growth and post-growth processing. This will, in general, result in different microstructures or different materials on the different array elements. Rapid thermal modulation, used to vary sensing kinetics, may also be useful to vary growth kinetics. At the same time, the use of microheaters for local control of film growth and processing

protects conventional silicon circuitry, which may be on the same chip, from elevated temperatures which now are only occurring only at the selected microhotplates. The electrical contact pads on each microhotplate may be used as an in situ characterization monitor of the growth and post-growth processes.

This article will present some examples of the different methods of metal oxide film growth that have been applied to microhotplate sensors. Examples include different methods of liquid deposition followed by sintering, evaporation, sputtering, and chemical vapor deposition (CVD). The latter method, because it best illustrates the variety of ways of using the microhotplate, will receive the greatest emphasis here. Preceding the discussion of oxide growth methods is a brief discussion of microhotplate fabrication.

2. Microhotplate Fabrication

Methods of producing microhotplates have been covered in review articles [17, 18] and will be briefly discussed here. An illustration of a four-element array of microhotplates is shown in Fig. 1 [19]. The device consists of a suspended platform that is only a few microns thick and has embedded in it a heater, thermometer and heat-spreading plate, and electrical contact pads to a sensing film that is deposited on top (Fig. 2). Essentially there are two common methods to produce a suspended hotplate with these functional layers. One technique uses topside micromachining in which first a sequence of process steps to define the layers mentioned above also defines trapezoidal openings through

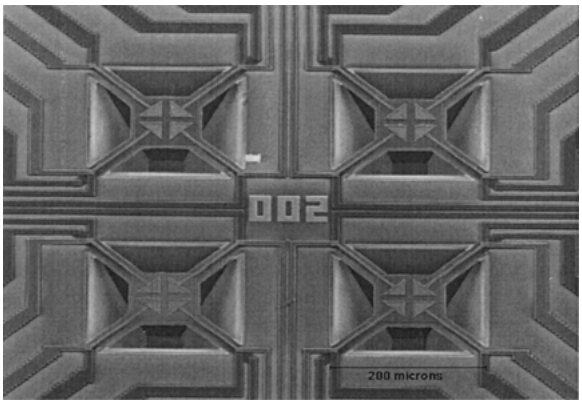

Fig. 1. Top: Scanning electron microscopy (SEM) image of a four-element array of microhotplates produced by top-surface micromachining.

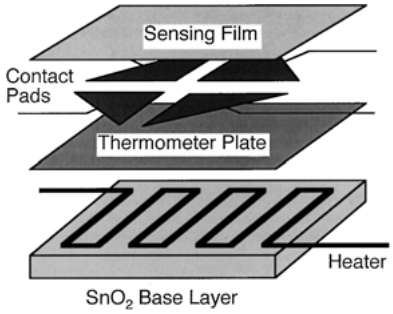

Fig. 2. Exploded view of the functional layers of microhotplate.

all oxide layers to the substrate silicon. This may be done in a CMOS process [3, 20]. Anisotropic etchants such as tetramethyl ammonium hydroxide (TMAH) or ethylene diamene pyrochatechol (EDP) or isotropic etchants such as xenon difluoride may be used etch the silicon starting at these openings and continuing until a pit is formed underneath the microhotplate. The layers in the microhotplate and legs are protected from the etch by oxide layers. A second technique uses a backside etch of the silicon to thin the substrate underneath the active layers (Fig. 3) [1, 2, 21]. The advantage of the backside etch is the surface remains flat for subsequent lithography steps. The advantage of the topside etch is that the processing is much more rapid, does not require backside alignment, and allows for the

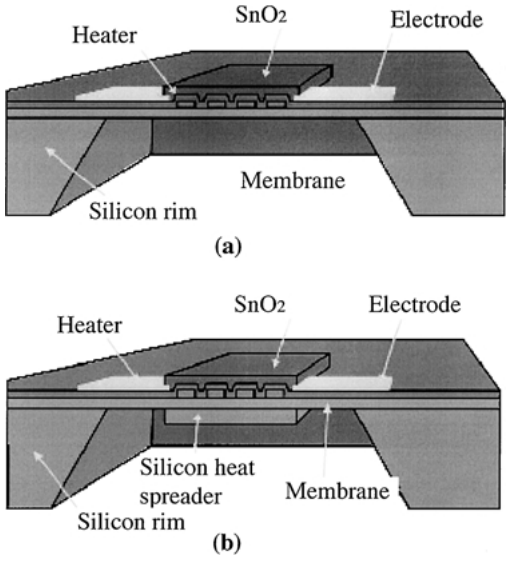

Fig. 3. Schematic of a backside etched microhotplate gas sensor: (a) without; (b) with silicon heat spreader under the active area [21].

production of smaller devices and denser arrays of separate microhotplates (because the lateral etch distance is much shorter).

3. Metal Oxide Film Deposition

The sensing performance of a metal oxide material depends strongly on its microstructure, with different forms of the same material having greatly different properties [18, 22–26]. Oxide film growth may be broken down into three categories, liquid phase deposition, physical vapor deposition, and chemical vapor deposition. Each of these methods may require elevated temperatures for growth or as a post-treatment. Utilization of the microhotplate heater to perform this function provides local control of stoichiometry, microstructure, or, in the case of CVD, the composition of the film.

3.1. Liquid Phase Deposition

The use of sintered pastes of metal oxides, sometimes mixed with catalysts, has been the most important fabrication method of discrete sensors dating to the original Taguchi patent [27]. Thick film versions of the device have been fabricated by screen printing pastes prepared from metal-oxide powder, inorganic additives and organic binders [28]. A key step in the fabrication process is sintering which electrically connects the metal oxide grains. The connections or "necks" provide high surface-to-volume regions where the conductivity may be modulated or intergrain contacts can produce Schottky barriers whose height is gas-sensitive [29, 30].

Figure 4 shows an example of a film deposited on a backside-etched microhotplate using a dropping technique [31]. A nanoparticle colloidal suspension synthesized by combining the decomposition of an organometallic precursor and controlled surface hydrolysis [32] was dropped onto an etched microhotplate. The microheater was used to heat the film to 500°C to produce the porous tin oxide material shown in Fig. 4(b). A low sintering temperature, compatible with the temperature range of the device, is possible due to the small size of the tin oxide particles. By performing the sensing film deposition after etching, dicing, and packaging, contamination of the sensing surface is avoided.

Puigcorbe et al. [33] describe a similar microdropping method using a different nanophase suspension.

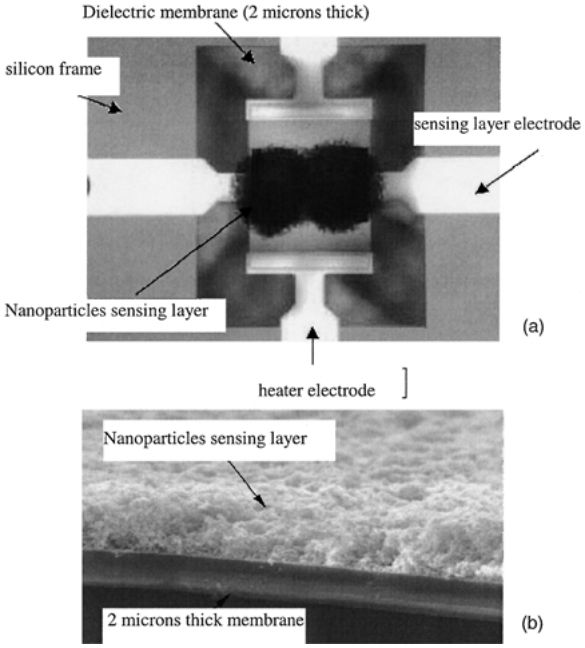

Fig. 4. (a) Top view of drop-deposited nanoparticle sensing layer. (b) SEM cross-sectional view of sensing layer [31].

The study explored the thermal mechanical properties of heated films on microhotplates and found that temperatures above 590°C resulted in cracks in the sensor. The films at 20 μm were about ten times thicker than the films of Fau et al. Strong thermal gradients at elevated operating temperatures produced deflections of the membrane, which ultimately produced the cracks. Capone et al. describe thick films prepared by dropping a Pd-doped SnO_2 paste onto a microhotplate. In this case the firing of the films was performed prior to packaging. By varying the doping level of Pd and using different contact geometry on different elements, an array of eight sensors was produced and then used to analyze mixtures of carbon monoxide and methane. Tsai et al. [34] used a two-step drop coating process: first a mixture of SnO_2, silica, and glycerol for adhesion, followed by a tin (II) 2-ethyl hexanoate, palladium acetate and 2-ethyl hexanoic acid mixture for sensing. The entire device was fired at 550°C for one hour. The device is shown in Fig. 5. A novel aspect of this work is that the functions of sensing and heating were both performed using this tin oxide film. Changes in CO concentration modified the conductance of the film, and thus the joule heating, leading to a temperature change. Oscillatory effects were observed under certain conditions due to this feedback mechanism.

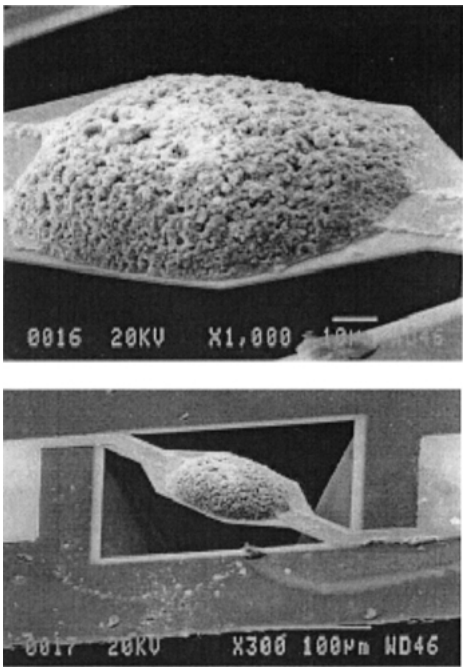

Fig. 5. SEM images of a microhotplate in which the drop coated sensing layer also acts as a heater [34].

A second method of applying liquid phase coatings to microhotplates is screen-printing. Vincenzi et al. applied a paste consisting of Pd catalyzed SnO_2 powder mixed with glass frit (to improve adhesion) in an organic vehicle to backside-etched microhotplates (Fig. 6) [35]. Screen printing usually involves applying some force to the substrate. Because of the fragility of the microhotplate membrane, a custom stencil was prepared for printing that featured a thicker, stiffer mask with a chamfered edge. The result was a 40 μm thick film of lateral dimension 250 μm located with an accuracy of 10 μm and with a spreading of 20 μm. The films were further processed with a curing step to remove the organics and a 750°C firing to sinter the material. Both heating the entire device in a furnace and using the microhotplate heater for heat treatment were tested, with the latter producing the higher yield.

Spin coating has been used to make thin (100 nm) films of nanoparticle-suspended films from a colloidal suspension [36]. The films were annealed at 500°C using the film's microheater resulting in a microstructure consisting of approximately 10 nm grains (Fig. 7). The deposition method is compatible with photoresist processing and also novel liftoff processing that uses the microheater. In that process a nitrocellulose coating is

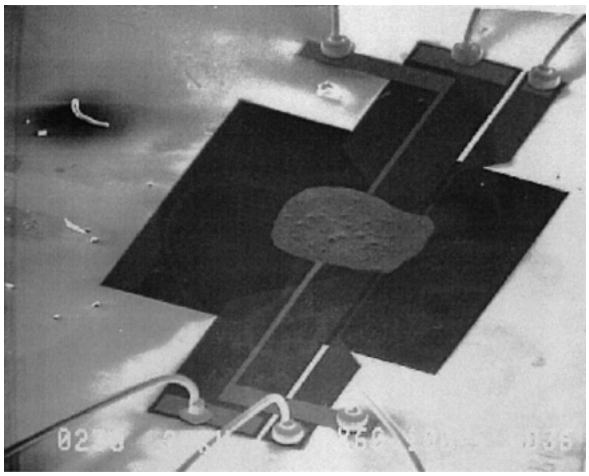

Fig. 6. SEM image of a screen printed thick film SnO_2 sensing layer on a Si_3N_4 membrane [35].

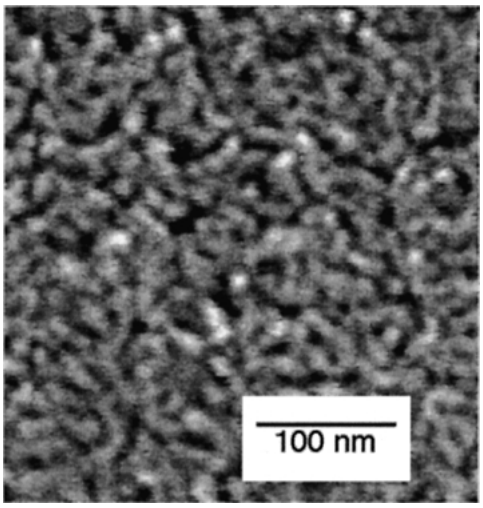

Fig. 7. Figure 2. SEM image of a nanoparticle film prepared by spin-coating [36].

removed using a 400°C pulse to the microhotplate prior to spinning on the metal oxide. A rinse in an organic solvent removes the remaining nitrocellulose, lifting off metal oxide everywhere except on the microhotplate.

3.2. Physical Vapor Deposition

Physical vapor deposition process offer advantages that may include cleaner vacuum-based process conditions, compatibility with lithographic techniques and thus more precise control of dimensions.

Reactive sputtering has been used to produce films with different microstructure on top-etched microhotplates (similar to Fig. 1) in which the array elements are set to different temperatures during the sputter process [15]. Figure 8 shows the microstructure from microhotplates set at 20°C, 300°C, and 500°C, where the grain size is observed to increase with growth temperature. Films deposited at room temperature were insulating, while heat-treated films were conducting.

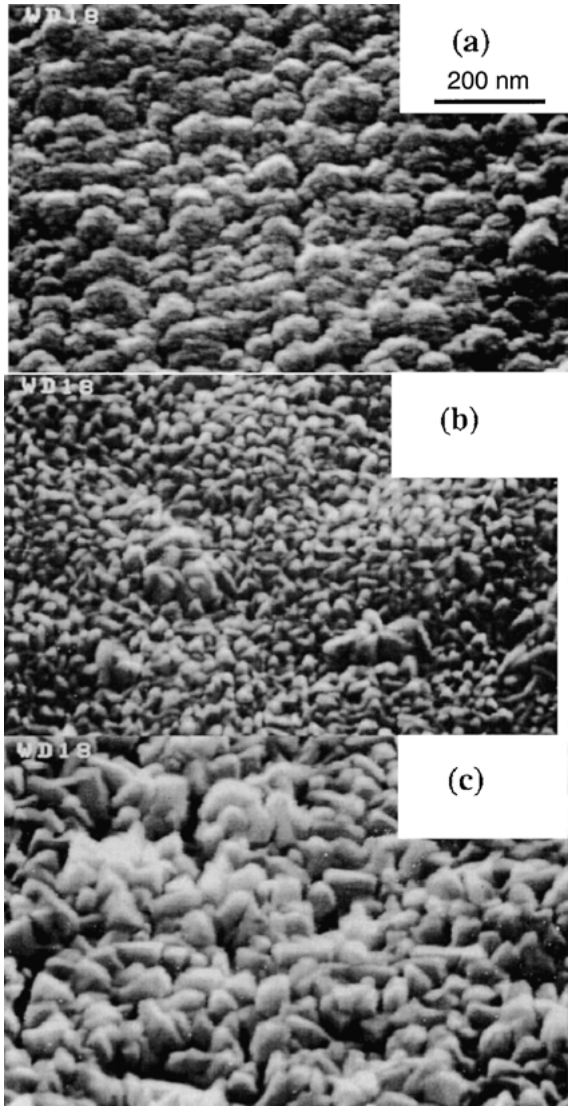

Fig. 8. (a) SEM images of SnO_2 grown on microsubstrates that were heated to three different temperatures during deposition: (a) room temperature, (b) 300°C, and (c) 500°C [15]. Magnification is the same for all three images.

Thus a lithography step to pattern the tin oxide was not necessary for operation of the devices. A similar effect was noted by Sheng et al. [37]. Chan et al. used lift-off to pattern sputtered tin oxide films grown on microhotplates [38]. Sintering was done using a furnace rather than the microheater and so they found it necessary to perform the process prior to defining contact metallizations.

Other methods reported for depositing metal oxides on microhotplates include electron beam deposition [10], and Rheotaxial Growth Thermal Oxidation (RGTO) [39] which involves depositing a metal such as Sn on a substrate heated above the melting temperature followed by a high temperature thermal oxidation process [40]. The anneal process was limited to 450°C and 500°C respectively in the two papers. These anneals were performed using ovens, although it would be possible to use the microheaters.

3.3. Chemical Vapor Deposition

Microhotplates can be used to selectively deposit a film on their heated surfaces using chemical vapor deposition methods [15, 41]. Figure 9 shows an example in which CVD tin oxide was deposited on a microhotplate heated to 450°C [42]. The organometallic reactant

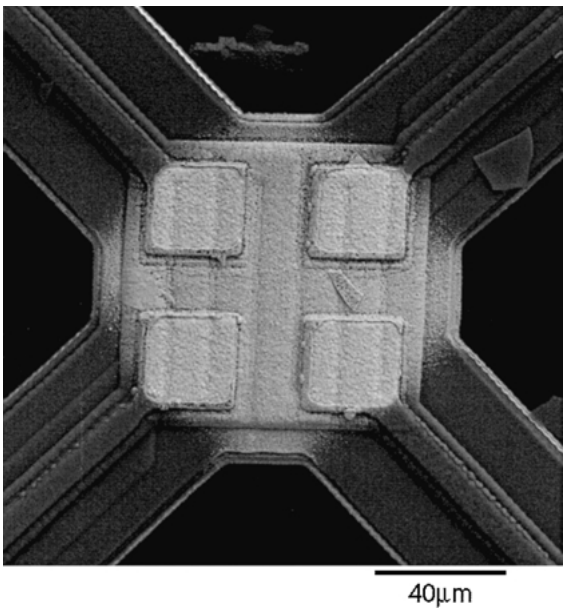

Fig. 9. SEM image of a CVD SnO_2 film grown on a microhotplate [42].

was provided by argon flowing through a tetramethyltin bubbler set to −45°C. This gas was diluted with argon and mixed with oxygen in room temperature apparatus. A range of process conditions of flow and pressure of the reactants have been explored [42, 43]. As is evident in the figure, the film only grows on the central part of the microhotplate that is above the temperature for nucleation and growth, the cooler parts along the legs of the microhotplate and the substrate are free of film.

This "self-lithography" characteristic, greatly simplifies the procedure for producing different films on different array elements as there is no need for photolithography. Benefits include a savings in the number of process steps with reduced contamination of the sensing layer and the ability to use high temperatures for growth without damaging more other components on the chip. Implementation of this approach combined with active CMOS circuits was recently demonstrated [44].

For studying metal oxide sensing films, combinatorial methods may be used with arrays of microhotplates. For example, to characterize the growth as a function of time, a set of array elements can be operated in the same CVD environment, at the same temperature, but for different growth times as in Fig. 10 [45]. Growth of TiO_2 films from titanium (IV) nitrate using array elements set to different growth temperatures and, for some elements, time-varying temperatures, has been characterized on a 16-element array [46]. Because of the low power of the microhotplate, it is also possible to operate the microhotplate in an environmental SEM containing the reactant gases and produce a movie of the growth process [47].

The CVD growth process consists of a nucleation process in which the accumulation rate is slow, followed by a more uniform growth rate once an appreciable fraction of the surface has been covered. This nucleation process can be controlled by different strategies. For example, in the growth of ZnO from diethyl zinc, DiMeo et al. [48] compared a film grown with a constant flow rate of reactant with a film grown with first a low concentration of reactant followed by the same higher flow rate as the first film. In each case the film growth was terminated when the film reached a fixed value of conductance (as will be discussed further in the next section.) Figure 11 shows the large difference in microstructure effected by the slow seeding process. The variations that could be produced by seeding with ultrathin metals was explored using arrays of 36 elements [49]. It was found that metal islands, formed by low coverage deposition and annealing, act as seeds, but that the size of the islands depended on the melting temperature of the metal. Low melting temperature metals produced larger seeds and

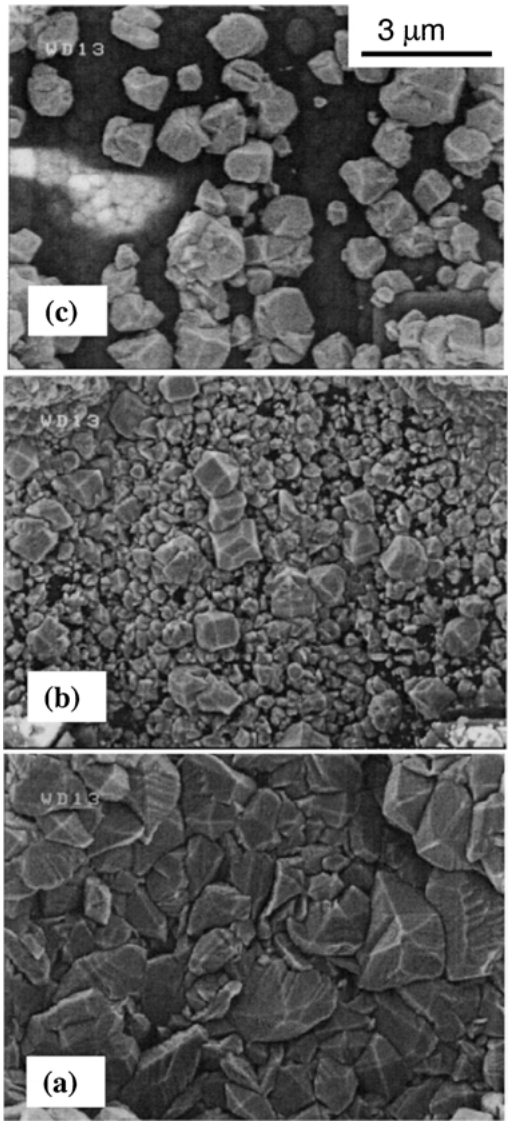

Fig. 10. SEM images of SnO_2 thin films deposited on microhotplates by CVD. The growth conditions were a hotplate temperature of 475°C, a tetramethyl tin bubbler temperature of −48°C with 8 sccm of carrier gas flow, a total pressure of 0.76 kPa, and a partial pressure of oxygen of 0.35 kPa. The images correspond to different elements of an array grown for different times: (a) 310 s where the grains are dispersed and mostly unconnected; (b) 510 s, where the density of grains has increased, but the substrate is still discernible through gaps in the film; and (c) 950 s where the film is fully connected across the microhotplate [45].

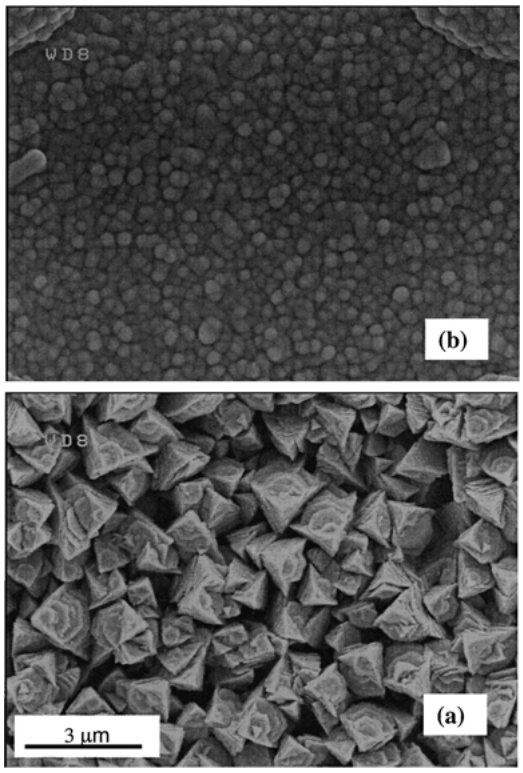

Fig. 11. SEM images of ZnO films grown by CVD from diethylzinc [48]. (a) Film growth proceeded at a constant flow rate of argon through the diethylzinc source; (b) film growth was in two stages, a one hour exposure to a low concentration of the precursor followed by a second stage using the same conditions as used to grow the film in (a). The first stage served to produce nucleation sites for ZnO growth.

thus larger grains. High sensitivity films were found by selecting metals that produced small seeds, resulting in fine-grained sensing films.

The rapid heating and cooling capabilities of microheaters may be used during CVD growth to alter the structure of films. Figure 12 shows a comparison of a film prepared under constant temperature heating with a film prepared using rapid pulsed heating. In this case the microheater was simply a 2 μm Pt line on the surface of an oxidized Si chip. Through application of a DC voltage to the line it was possible to raise the temperature to 350°C on the line. Performed in the presence of tin nitrate, the film shown in Fig. 12(a) was grown. The film in Fig. 12(b) was obtained under the same flow conditions, with, instead, a pulsed heating consisting of 8 μs pulses to the same temperature, repeated at 10 kHz. For very short pulses with low duty cycle, the heating and cooling time constant

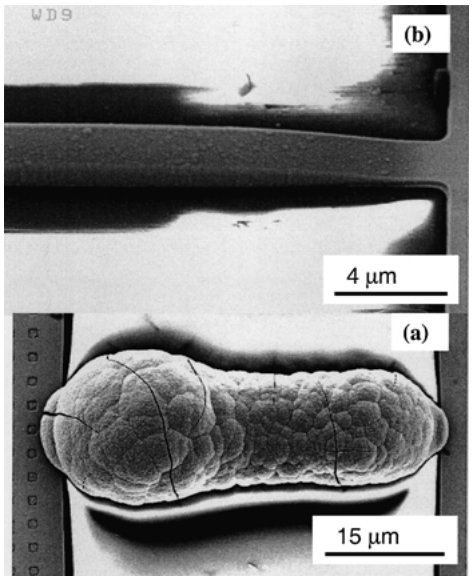

Fig. 12. SEM images of CVD films grown on a Pt line on a Si substrate using (a) constant temperature heating, (b) pulsed heating using 8 μs voltage pulses repeated at 10 kHz [50].

of the metal line (as measured by the resistance transient) was measured to be about 1 μs. At higher duty cycles, the silicon substrate cannot effectively remove heat, resulting in a longer, nonexponential cooldown. As is evident from the figure the gross morphology of the film is markedly different, due to the different reactant transport mechanisms that are operative under the two different timescales of growth [50].

4. *In Situ* Electrical Characterization

Conventionally in CVD, it is difficult to monitor the progress of the growing film, and often the process relies on reproducible conditions and timing. The built-in contacts on the microhotplate allow measurement of the sensing film as it is growing and termination of the growth by switching off the heater at a precisely specified conductance value [15]. This *in situ* monitoring allows for more detailed characterization of the growth process. It also allows termination of the growth when a desired conductance is reached, improving process repeatability.

Figure 13 shows the conductance measured during the CVD growth of SnO_2 on five elements of a 36-element array [19]. These elements were prepared with an initial "seed" layer of 16 Å Co. Growth temperature

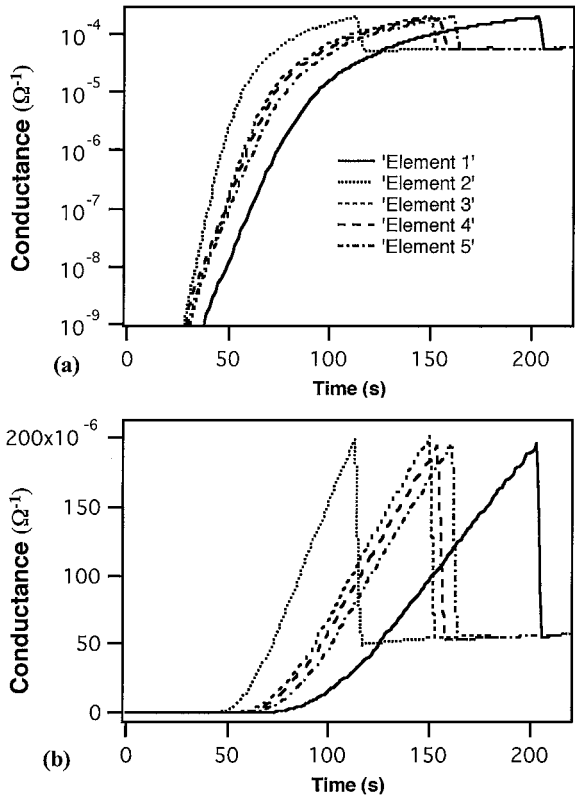

Fig. 13. Conductance measurements during the CVD growth of SnO_2 on five Co seeded array elements [19]. Seeding layer thickness was 16 Å on each element. (a) Data shown on a log scale, showing initial nucleation. (b) Data on a linear scale, showing the linear increase in conductance with time at longer times.

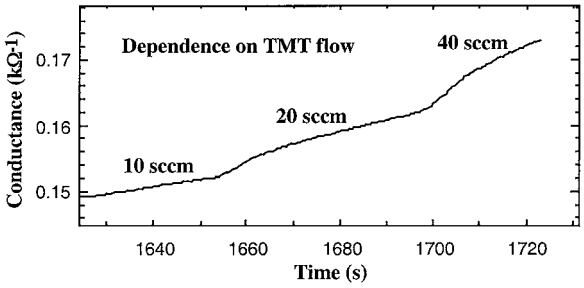

Fig. 14. Film conductance measured during OMCVD growth with varying tetramethyltin flow [15].

was set to 500°C. Growth was stopped on a particular microhotplate by turning off its heater when the film resistance reached 5 kΩ. This resulted in sensing films with final resistances that were within about five percent the average. The log-scale plot (Fig. 13(a)) makes clear the initial stages of growth from which one can define a nucleation time as the interval between the switching on of the heater and the onset of measurable (resistance <1 GΩ) electrical conductance. The log-scale plot also shows the rapid rise in conductance associated with the formation of a continuous film. The linear plot shows a linear increase in conductance with time for time greater than about half the growth time. Because conductance is directly proportional to thickness for a continuous film of uniform composition, this suggests a constant growth rate was attained. Using calibrated wavelength dispersive spectroscopy measurements, a conversion from time-dependent conductance to film thickness has been demonstrated [45]. It was noted that accurate conversion requires taking into account the stoichiometry of the growing film, which must be determined for each set of gas process conditions.

Changes in the process conditions during growth can be detected by the electrical measurements on the film. Figure 14 shows the changes observed during conductance monitoring of tin oxide growth from TMT and oxygen when the flow of argon was increased through the TMT bubbler [15]. Higher partial pressures of the reactive gas produced faster rates of increase in the conductance. The transient conductance rises between linear regimes in this plot were attributed to transients in the flow controller. During zinc oxide growth from diethyl zinc, Dimeo et al. observed millisecond scale oscillations in the conductance data, which was shown to be due to oscillations in the gas concentration caused by a faulty mass flow controller [45]. Figure 15 shows the electrical signal from the mass flow controller and the conductance data obtained using an oscilloscope. These oscillations were observed as a small modulation of a generally rising conductance curve like that in Fig. 13. Note that the conductance does not show periodic stair-like rises as might be expected for a simple modulation in growth rate, but actually a part of the waveform has negative slope. In this situation, the growing film is acting like a gas sensor, detecting changes in the oxygen to diethylzinc ratio. A 5 ms phase lag between the maxima of the signals was attributed to the time required to flow from the mass flow controller to the sample. Other effects, such as the release of bubbles in a bubbler or the switching on and off of neighboring microhotplates in an array [51], can produce similar modulations in gas concentration which can be detected through conductance monitoring.

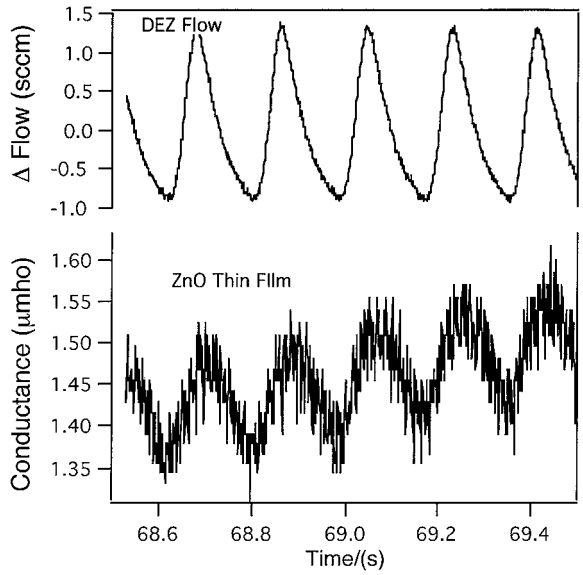

Fig. 15. Rapid oscillations in conductance during CVD growth of ZnO using diethylzinc [45]. Lower panel is conductance vs time data collected using an oscilloscope, and the upper panel is the simultaneously acquired signal taken from the mass flow controller that regulates the flow over the DEZ.

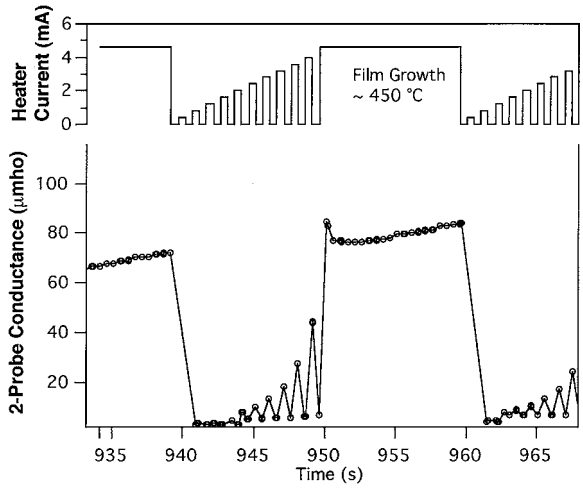

Fig. 16. Probe of conductance at different temperatures using intermittent cycles of pulsed heating during CVD growth of tin oxide on a microhotplate [43]. Upper panel shows heater current schedule. Lower panel shows conductance vs time.

More detailed electrical information can be obtained during growth by intermittently pulsing the temperature to different values [15]. Figure 16 is an example in which intermittent measurements of the temperature-dependent film conductance were performed during CVD growth [43]. The temperatures used during the characterization part of the cycle were kept below the temperature necessary for growth. The temperature dependent resistance can be used to differentiate films which have a similar conductance but different stoichiometry due to changes in process condition.

References

1. V. Demarne and A. Grisel, *Sensors and Actuators*, **13**, 301 (1988).
2. U. Dibbern, *Sensors and Actuators B-Chemical*, **2**, 63 (1990).
3. J. Suehle, R. Cavicchi, M. Gaitan, and S. Semancik, *IEEE Electron Device Lett.*, **14**, 118 (1993).
4. N.R. Swart and A. Nathan, *Sensors and Actuators a-Physical*, **43**, 3 (1994).
5. W.Y. Chung, C.H. Shim, S.D. Choi, and D.D. Lee, *Sensors and Actuators B-Chemical*, **20**, 139 (1994).
6. H.E. Endres, W. Gottler, R. Hartinger, S. Drost, W. Hellmich, G. Muller, C. BoschvonBraunmuhl, A. Krenkow, C. Perego, and G. Sberveglieri, *Sensors and Actuators B-Chemical*, **36**, 353 (1996).
7. B. Panchapakesan, D. DeVoe, R.E. Cavicchi, and S. Semancik, *Mat. Res. Soc. Symp. Proc.*, **574**, 213 (2000).
8. C. Cane, I. Gracia, A. Gotz, L. Fonseca, E. Lora-Tamayo, M.C. Horrillo, I. Sayago, J.I. Robla, J. Rodrigo, and J. Gutierrez, *Sensors and Actuators B-Chemical*, **65**, 244 (2000).
9. S. Capone, P. Siciliano, N. Barsan, U. Weimar, and L. Vasanelli, *Sensors and Actuators B-Chemical*, **78**, 40 (2001).
10. Y.W. Mo, Y. Okawa, M. Tajima, T. Nakai, N. Yoshiike, and K. Natukawa, *Sensors and Actuators B-Chemical*, **79**, 175 (2001).
11. R.E. Cavicchi, J.S. Suehle, K.G. Kreider, M. Gaitan, and P. Chaparala, *IEEE Electron Device Lett.*, **16**, 286 (1995).
12. A. Heilig, N. Barsan, U. Weimar, M. Schweizer-Berberich, J.W. Gardner, and W. Gopel, *Sensors and Actuators B-Chemical*, **43**, 45 (1997).
13. D. Barrettino, M. Graf, M.M. Zimmermann, A. Hierlemann, H. Baltes, S. Hahn, N. Barsan, and U. Weimar, in *IEEE International Symposium on Circuits and Systems (ISCAS), 2002.* (Institute of Electrical and Electronics Engineers Inc., Phoenix, AZ, 2002), vol. 2, p. 157.
14. A.R. Hefner, D.W. Berning, M.E. Zaghloul, J.S. Suehle, M. Afridi, R.E. Cavicchi, and S. Semancik, in *IEEE International Symposium on Circuits and Systems (ISCAS), 2002.* (Institute of Electrical and Electronics Engineers Inc., Phoenix, AZ, 2002), vol. 2, p. 732.
15. R.E. Cavicchi, J.S. Suehle, K.G. Kreider, J.A. Small, M. Gaitan, and P. Chaparala, *Appl. Phys. Lett.*, **66**, 812 (1995).
16. S. Semancik and R.E. Cavicchi, *Acc. Chem. Res.*, **31**, 279 (1998).
17. H.L. Tuller and R. Mlcak, *Journal of Electroceramics*, **4**, 415 (2000).
18. T. Simon, N. Barsan, M. Bauer, and U. Weimar, *Sensors and Actuators B-Chemical*, **73**, 1 (2001).
19. R.E. Cavicchi, S. Semancik, R.M. Walton, B. Panchapakesan, D.L. DeVoe, M.I. Aquino-Class, J.D. Allen, and J.S. Suehle, in *Chemical Microsensors and Applications II*, edited by S. Buettgenbach (SPIE-The International Society for Optical Engineering, Boston, MA, 1999), vol. Proc. SPIE 3857, p. 38.

20. J.C. Marshall, M. Parameswaran, M.E. Zaghloul, and M. Gaitan, *IEEE Circuits and Devices*, **8**, 10 (1992).
21. I. Gracia, J. Santander, C. Cane, M.C. Horrillo, I. Sayago, and J. Gutierrez, *Sensors and Actuators B-Chemical*, **77**, 409 (2001). Figure 3 reprinted with permission from Elsevier Science
22. J.F. McAleer, P.T. Moseley, J.O.W. Norris, and D.E. Williams, *J. Chem. Soc. Faraday Trans.*, **83**, 1323 (1987).
23. D. Kohl, *Sensors and Actuators*, **18**, 71 (1989).
24. N. Yamazoe, in *3rd International Meeting on Chemical Sensors* (Cleveland, 1990), p. 3.
25. C. Xu, J. Tamaki, N. Miura, and N. Yamazoe, *Sensors and Actuators B*, **3**, 147 (1991).
26. A. Balasubramanian, *Solid State Phenomena*, **55**, 54 (1997).
27. N. Taguchi, United Kingdom Patent Specification 1280809.
28. G. Martinelli and M.C. Carotta, *Sensors and Actuators B-Chemical*, **23**, 157 (1995).
29. P.T. Moseley and D.E. Williams, in *Adam Hilger Series on Sensors*, edited by P.T. Moseley (IOP Publishing Ltd, Bristol, England, 1991), p. 46.
30. J. Janata, *Principles of Chemical Sensors* (Plenum Press, NY, 1992).
31. P. Fau, M. Sauvan, S. Trautweiler, C. Nayral, L. Erades, A. Maisonnat, and B. Chaudret, *Sensors and Actuators B-Chemical*, **78**, 83 (2001). Figure 4 reprinted with permission from Elsevier Science
32. C. Nayral, T. Ould-Ely, A. Maisonnat, B. Chaudret, P. Fau, L. Lescouzeres, and A. Peyre-Lavigne, *Advanced Materials*, **11**, 61 (1999).
33. J. Puigcorbe, A. Vila, J. Cerda, A. Cirera, I. Gracia, C. Cane, and J.R. Morante, *Sensors and Actuators a-Physical*, **97/98**, 379 (2002).
34. P.P. Tsai, I.C. Chen, and C.J. Ho, *Sensors and Actuators B-Chemical*, **76**, 380 (2001). Figure 5 reprinted with permission from Elsevier Science.
35. D. Vincenzi, M.A. Butturi, V. Guidi, M.C. Carotta, G. Martinelli, V. Guarnieri, S. Brida, B. Margesin, F. Giacomozzi, M. Zen, D. Giusti, G. Soncini, A.A. Vasiliev, and A.V. Pisliakov, *Journal of Vacuum Science & Technology B*, **18**, 2441 (2000).
36. R.E. Cavicchi, R.M. Walton, J.D. Allen, M. Aquino-Class, and B. Panchapakesan, *Sensors and Actuators B: Chemical*, **77**, 145 (2001).
37. L.Y. Sheng, Z.N. Tang, J. Wu, P.C.H. Chan, and J.K.O. Sin, *Sensors and Actuators B-Chemical*, **49**, 81 (1998).
38. P.C.H. Chan, G.Z. Yan, L.Y. Sheng, R.K. Sharma, Z. Tang, J.K.O. Sin, I.M. Hsing, and Y. Wang, *Sensors and Actuators B-Chemical*, **82**, 277 (2002).
39. V. Guidi, M.A. Butturi, M.C. Carotta, B. Cavicchi, M. Ferroni, C. Malagu, G. Martinelli, D. Vincenzi, M. Sacerdoti, and M. Zen, *Sensors and Actuators B-Chemical*, **84**, 72 (2002).
40. G. Sberveglieri, G. Faglia, S. Groppelli, P. Nelli, and A. Camanzi, *Semiconductor Science Technology*, **5**, 1231 (1990).
41. S. Majoo, J.W. Schwank, J.L. Gland, and K.D. Wise, *IEEE Electron Device Letters*, **16**, 217 (1995).
42. F. Dimeo, Jr., S. Semancik, R.E. Cavicchi, J.S. Suehle, N.H. Tea, M.D. Vaudin, and J.T. Kelliher, in *Proceedings of the 1996 MRS Fall Meeting* (Boston, MA, 1997), vol. 444, p. 203.
43. F. Dimeo, Jr., S. Semancik, R.E. Cavicchi, J.S. Suehle, P. Chaparala, and N.H. Tea, in *Proceedings of the 1995 MRS Fall Meeting* (Boston, MA, 1996), vol. 415, p. 231.
44. M. Afridi, J.S. Suehle, M.E. Zaghloul, R.E. Cavicchi, and S. Semancik, in *European Conference on Circuit Theory and Design, August 28–31* (Espoo, Finland, 2001).
45. F. DiMeo, R.E. Cavicchi, S. Semancik, J.S. Suehle, N.H. Tea, J. Small, J. Armstrong, and J.T. Kelliher, *J. Vac. Sci. Technol. A*, **16**, 131 (1998).
46. C.J. Taylor and S. Semancik, *Chemistry of Materials*, **14**, 1671 (2002).
47. S.A. Wight, R.E. Cavicchi, and M.J. Nystrom, *Review of Scientific Instruments* (submitted in 2002).
48. F. DiMeo, Jr., R.E. Cavicchi, S. Semancik, J.S. Suehle, N.H. Tea, and J.T. Kelliher, in *Proceedings of the 1996 MRS Fall Meeting* (Boston, MA, 1997), vol. 441, p. 69.
49. B. Panchepakesan, D.L. Devoe, M. Widmaeir, R.E. Cavicchi, and S. Semancik, *Nanotechnology*, **12**, 336 (2001).
50. C. Taylor and R.E. Cavicchi (unpublished).
51. J. Tiffany, R.E. Cavicchi, and S. Semancik, in *Advanced Environmental and Chemical Sensing Technology*, edited by S. Butettgenbach (2000), vol. 4205, p. 240.